Design of 5G Full Dimension Massive MIMO Systems

Qurrat-Ul-Ain Nadeem, Abla Kammoun, Merouane Debbah, Mohamed-Slim Alouini

Design of 5G Full Dimension Massive MIMO Systems

Qurrat-Ul-Ain Nadeem, *Student Member, IEEE,* Abla Kammoun, *Member, IEEE,* Mérouane Debbah, *Fellow, IEEE,* and Mohamed-Slim Alouini, *Fellow, IEEE*

Abstract

Massive multiple-input-multiple-output (MIMO) transmission is a promising technology to improve the capacity and reliability of wireless systems. However, the number of antennas that can be equipped at a base station (BS) is limited by the BS form factor, posing a challenge to the deployment of massive linear arrays. To cope with this limitation, this work discusses Full Dimension MIMO (FD-MIMO), which is currently an active area of research and standardization in the 3rd Generation Partnership Project (3GPP) for evolution towards fifth generation (5G) cellular systems. FD-MIMO utilizes an active antenna system (AAS) with a 2D planar array structure, which provides the ability of adaptive electronic beamforming in the 3D space. This paper presents the design of the AAS and the ongoing efforts in the 3GPP to develop the corresponding 3D channel model. Compact structure of large-scale antenna arrays drastically increases the spatial correlation in FD-MIMO systems. In order to account for its effects, the generalized spatial correlation functions for channels constituted by individual antenna elements and overall antenna ports in the AAS are derived. Exploiting the quasi-static channel covariance matrices of the users, the problem of determining the optimal downtilt weight vector for antenna ports, which maximizes the minimum signal-to-interference ratio of a multi-user multiple-input-single-output system, is formulated as a fractional optimization problem. A quasi-optimal solution is obtained through the application of semi-definite relaxation and Dinkelbach's method. Finally, the user-group specific elevation beamforming scenario is devised, which offers significant performance gains as confirmed through simulations. These results have direct application in the analysis of 5G FD-MIMO systems.

Index Terms

Manuscript received December 9, 2016. A part of this work has been accepted for publication in IEEE Global Communications Conference, Washington DC, USA, Dec. 2016.

Q.-U.-A. Nadeem, A. Kammoun and M.-S. Alouini are with the Computer, Electrical, and Mathematical Sciences and Engineering (CEMSE) Division, King Abdullah University of Science and Technology (KAUST), Thuwal, Makkah Province, Saudi Arabia. (e-mail: {qurratulain.nadeem,abla.kammoun,slim.alouini}@kaust.edu.sa)

M. Debbah is with Supélec, Gif-sur-Yvette, France and Mathematical and Algorithmic Sciences Lab, Huawei France R&D, Paris, France (e-mail: merouane.debbah@huawei.com, merouane.debbah@supelec.fr).

Full Dimension multiple-input-multiple-output (FD-MIMO), elevation beamforming, downtilt, 3rd Generation Partnership Project (3GPP), fifth generation (5G), active antenna system (AAS).

I. Introduction

Multiple-input multiple-output (MIMO) technology has remained a subject of interest in the last two decades due to its ability to cope with the increase in the wireless data traffic. In order to be compatible with the existing 3rd Generation Partnership Project (3GPP) Long Term Evolution (LTE) standard, most of the existing MIMO implementations consider the deployment of fewer than ten linearly placed antennas at the base station (BS) [1]. The corresponding improvement in spectral efficiency, although important, is still relatively modest and can be vastly improved by scaling up these systems by orders of magnitude. This has led to the introduction of massive MIMO systems, where each BS is equipped with a large number of antennas, allowing it to serve many users in the same time-frequency resource using linear precoding methods [2]–[4].

While massive MIMO technology is a key enabler for next generation cellular systems, there are still many practical challenges down the road to its successful deployment [2], [4]. One of the main challenges is that the number of antennas that can be equipped at the top of the BS tower is limited by the BS form factor and operating LTE carrier frequency. To circumvent this problem, some efforts have been made in the 3GPP to come up with practical implementations of massive MIMO systems. As a starting point, the use of a 2D uniform planar array has been proposed, which can be readily installed in practice as compared to the conventional uniformly spaced linear array [5]–[7]. For example, a 16×16 half wavelength spaced 2D uniform planar array occupies about $1\text{m}\times 1\text{m}$ space at a typical LTE carrier frequency of 2.5 GHz. By contrast, about 15m spacing is required in the horizontal direction to install a linear array of 256 antennas.

In addition to the emergence of large-scale antenna arrays, the cell site architecture itself has evolved in the last decade from the one wherein the base transceiver station (BTS) equipment is located away from the passive antenna element array, to the one wherein the analogue portion of the BTS, comprising of amplifiers, phase shifters and other active transceiver components, is located in the remote radio head closer to the passive antennas. The next stage is the integration of the active transceiver unit array into the passive antenna element array, resulting in an active antenna system (AAS) [8], [9]. The AAS can support adaptive electronic beamforming by controlling the phase and amplitude weights applied to individual antenna elements. The use of an AAS with a 2D planar array structure results in full dimension (FD) MIMO, which was

identified as a promising technology for 5G cellular systems in 3GPP Release-12 [10]. Follow-up study items are under completion [11] and formal standardization will be done in Release-13.

FD-MIMO has two important distinguishing features as compared to the conventional LTE systems. Firstly, the number of antennas supported within a feasible BS form factor has increased. Secondly, the 2D arrangement of active antenna elements provides the ability of adaptive electronic beam control over both the elevation and the traditional azimuth dimensions [12], [13]. These elements are organized into antenna ports, where each port is mapped to a group of physical antenna elements arranged in the vertical direction [7]. Controlling the phase, amplitude and delay of these individual elements allows for the dynamic adaptation of the vertical dimension of the antenna port radiation pattern, resulting in an electric downtilt feature [8], [9], [14]. Popularly known as elevation beamforming, this technique can help realize more directed and spatially separated transmissions to a large number of users [15], [16]. In order to facilitate the evaluation of FD-MIMO techniques, a large effort in 3D channel modeling is needed. The 3GPP has recently outlined a 3D channel model in [6], which now forms the basis of most studies on FD-MIMO.

The additional control over the elevation dimension enables a variety of strategies such as sector-specific and user-specific elevation beamforming, and cell splitting [12], [17], [18]. The authors in [16] used lab and field trials to show that 3D beamforming can achieve significant performance gains in real indoor and outdoor deployments, by adapting the vertical dimension of the antenna port radiation pattern at the BS individually for each user according to its location. Some 3D beamforming designs were proposed in [14] for a single user multiple-input-single-output (MISO) system, wherein the authors used the approximate antenna port radiation pattern expressions proposed in [19], [20] to find the optimal downtilt angle. This approach, also used in works dealing with multi-user scenarios [21], [22], discards the role played by physical antenna elements constituting an antenna port in performing the downtilt. The actual radiation pattern of a port depends on the number of elements constituting it, their patterns, relative positions and corresponding weights [7], [11]. More sophisticated elevation beamforming methods need to be developed that take into account the underlying physical construction of the antenna port.

The compact structure of large-scale antenna arrays and the small values of elevation angular spread in realistic propagation environments drastically increase the spatial correlation in FD-MIMO systems, making it imperative to account for it while studying the performance benefits of elevation beamforming techniques. There have been some works that study spatial correlation in 3D propagation scenarios [23]–[26]. An important contribution appears in [24], wherein the

authors developed closed-form expressions for the spatial correlation and large system ergodic mutual information (MI) for a 3D cross-polarized channel model, assuming the angles to follow Von Mises (VM) distribution. The authors in [23] expressed correlation in a closed-form as a function of angular and array parameters for several antenna arrays and used the developed covariance matrices to study the impact of angular spreads on the system capacity. However, these works consider passive omnidirectional antenna elements arranged in the azimuth plane only, and the correlation analysis is done for only specific forms of underlying angular distributions.

This paper introduces the design of the 2D planar active antenna array, which plays a key role in the implementation of FD-MIMO systems. The array constitutes of columns of active antenna elements, where each column is referred to as an antenna port and is fed with a corresponding downtilt weight vector to steer the vertical radiation pattern of that port in the targeted direction. For the analysis of these systems, the 3D channel model outlined in the 3GPP technical report (TR) 36.873 [6] is introduced and explained. In our study of FD-MIMO systems, we make two main contributions. Firstly, the exact spatial correlation function (SCF) for the FD channels constituted by individual antenna elements in the array is derived in **Theorem 1**, exploiting the spherical harmonic expansion (SHE) of plane waves. The final analytical expression depends on the angular parameters and the geometry of the array through the Fourier series (FS) coefficients of the power spectra, and can be used for any arbitrary 3D propagation environment. The correlation between the ports is then expressed as a function of the correlation matrix of the elements constituting the ports and the downtilt weight vectors. The second contribution is to devise efficient elevation beamforming algorithms that optimize these weight vectors, utilizing the quasi-static channel covariance matrices of the users obtained from the derived SCF, and thereby releasing the high dependence on the instantaneous channel state information. The closed-form expression for the signal-to-noise ratio (SNR) maximizing weight vectors for the single user MISO system is given in **Theorem 2**. The downlink of a multi-user MISO system is studied next under the assumption that all antenna ports transmit using a single optimal downtilt weight vector. The problem of determining this vector that maximizes the minimum signal-to-interference ratio (SIR) of the system is formulated as a fractional optimization problem, for which a quasi-optimal solution is obtained through the application of semi-definite relaxation and Dinkelbach's method. Finally, we devise a user-group specific elevation beamforming scenario, wherein the user population is partitioned into groups based on the users' channel covariance matrices and each user-group is served by a subset of ports which transmit using an optimal downtilt weight

vector. Simulations results show that even the single optimal downtilt beamforming scenario yields significant performance gains, while the user-group specific beamforming is even more effective. The derived results are directly applicable to the analysis of 5G FD-MIMO systems.

The rest of this article is organized as follows. Section II discusses the design of the 2D AAS for FD-MIMO implementation and presents the corresponding 3GPP 3D channel model. In section III, the exact SCFs for channels constituted by individual antenna elements and the overall antenna ports are derived. Section IV presents the elevation beamforming algorithms that optimize the downtilt weight vectors of the antenna ports in the single user and multi-user MISO settings. User-group specific elevation beamforming scenario is devised in section V. Section VI provides simulation results and finally, in section VII some concluding remarks are drawn.

II. Two-dimensional Active Antenna Array and 3D Channel Model

The idea of exploiting the elevation domain of the channel for performance optimization has led to the development of FD-MIMO systems. In fact, several field trials results have shown that the arrangement of active antenna elements in the vertical dimension provides additional degrees of freedom that can be exploited to form multiple elevation domain beams, resulting in significant performance gains [16], [27]. Most commercial solutions, however, deploy a smaller set of antennas arranged in the horizontal domain only, to be compatible with the existing LTE standards. The recent 3GPP reports on FD-MIMO envision that an AAS, utilizing a large number of antenna elements arranged in a 2D planar array structure, can be designed to realize spatially separated transmission links to a large number of users. In this section, we introduce this 2D AAS and outline the corresponding 3GPP FD-MIMO channel model.

A. Active Antenna Array for FD-MIMO

In order to realize the performance benefits of FD-MIMO techniques, an efficient implementation of an AAS with a 2D planar array structure is a key requirement. The AAS is an advanced BS technology, which integrates the active transceiver unit array into the passive antenna element array, allowing the gain, beamwidth and downtilt of the transmit beam to be controlled adaptively by active electronic components connected directly to each element [8], [9]. These active antenna elements should be placed in both the vertical and horizontal directions to provide the ability of adaptive electronic beamforming in the elevation and the traditional azimuth dimensions. In doing so, the array should also have a form factor that is adequate for actual deployments.

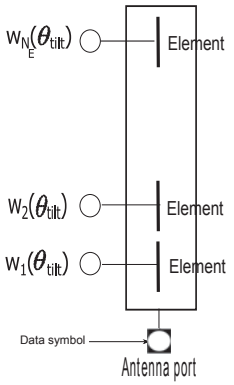

Fig. 1. Antenna port.

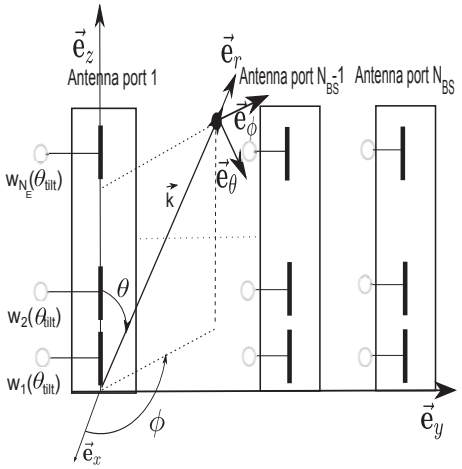

Fig. 2. Active antenna array.

The 3GPP proposes the organization of the radio resource on the basis of antenna ports, where each port is mapped to a group of physical antenna elements arranged in the vertical domain. The elements in a port carry the same signal and are fed with corresponding downtilt weights to focus the wavefront in the direction of the targeted user. The structure of a typical antenna port is shown in Fig. 1. Several such ports can be arranged in the horizontal and vertical directions to serve digitally precoded signals to different users at different downtilt angles in the same time-frequency slot. The higher is the number of vertically stacked elements in a port, the narrower is the transmitted beam. This work configures the entire column of elements as a port.

A generic AAS architecture as defined in section V of the 3GPP TR37.840 [7] takes a 2D planar array structure for the antenna elements. Each antenna port comprises of N_E antenna elements arranged along the $\hat{\mathbf{e}}_z$ direction. There are N_{BS} such ports placed at equidistant positions in the $\hat{\mathbf{e}}_y$ direction, where the downtilt angle, θ_{tilt}, of the radiation pattern of every port is controlled through the weights $w_k(\theta_{tilt})$, $k = 1, \ldots, N_E$. The resulting configuration for vertically polarized elements is shown in Fig. 2. The form factor for an 8×8 array with 0.5λ inter-port and inter-element spacing at 2.5 GHz LTE frequency is $0.5m \times 0.5m$, which is quite practical.

B. Antenna Element Approach towards 3D Channel Modeling

Preliminary studies on 3D channel modeling consider the channels between the overall antenna ports rather than between the physical elements constituting these ports and use the approximate antenna port radiation pattern expression proposed in [19], [20]. The focus of the ongoing 3GPP's standardization efforts is to develop a 3D channel model that takes into account the geometry

and properties of the individual elements constituting the AAS. The resulting model introduced in TR 36.873 [6], has not been utilized exactly in theoretical works on FD-MIMO so far.

In theory, the global radiation pattern of an antenna port depends on the positions and number of the antenna elements within it, their patterns and corresponding weights. In other words, the antenna port radiation pattern is created by the superposition of the element radiation pattern and the array factor for that port, where the element radiation pattern is given by [6], [7],

$$A_E(\phi,\theta) = G_{E,max} - \min\{-(A_{E,H}(\phi) + A_{E,V}(\theta)), A_m\}, \quad \text{where,} \tag{1}$$

$$A_{E,H}(\phi) = -\min\left[12\left(\frac{\phi}{\phi_{3dB}}\right)^2, A_m\right] \text{dB}, \tag{2}$$

$$A_{E,V}(\theta) = -\min\left[12\left(\frac{\theta-\frac{\pi}{2}}{\theta_{3dB}}\right)^2, SLA_v\right] \text{dB}, \tag{3}$$

where ϕ and θ denote the azimuth and elevation angles respectively, $A_{E,H}(\phi)$ and $A_{E,V}(\theta)$ are the radiation patterns in the horizontal and vertical directions respectively, $G_{E,max}$ is the maximum directional element gain, ϕ_{3dB} and θ_{3dB} are the half power beamwidths in the azimuth and elevation domains respectively, A_m is the maximum attenuation and SLA_v is the vertical side lobe attenuation level. The global field pattern of a vertically polarized element in linear scale is $\sqrt{10^{\frac{G_{E,max}}{10}}}\mathrm{g}_E(\phi,\theta)$, where $g_E(\phi,\theta) \approx g_{E,H}(\phi)g_{E,V}(\theta)$ with,

$$g_{E,H}(\phi) = \exp\left(-1.2\left(\frac{\phi}{\phi_{3dB}}\right)^2 \ln 10\right), \tag{4}$$

$$g_{E,V}(\theta) = \exp\left(-1.2\left(\frac{\theta-\frac{\pi}{2}}{\theta_{3dB}}\right)^2 \ln 10\right). \tag{5}$$

The overall array radiation pattern is a function of this individual element radiation pattern and the array factor matrix, **A**, for the AAS given by [7],

$$\mathbf{A} = \mathbf{W} \circ \mathbf{V}, \tag{6}$$

where $\circ$ is the Hadamard product, **V** is a $N_E \times N_{BS}$ matrix containing the array responses of the individual radiation elements with each entry given by,

$$[\mathbf{V}]_{k,s} = \exp(i\mathbf{k}.\mathbf{x}_{k,s}),\ k = 1,\ldots,N_E, s = 1,\ldots,N_{BS}, \tag{7}$$

where **.** is the scalar dot product, $\mathbf{x}_{k,s}$ is the location vector of the k^{th} antenna element in the s^{th} Tx antenna port, and **k** is the Tx wave vector, where $\mathbf{k} = \frac{2\pi}{\lambda}\hat{\mathbf{v}}$, with $\hat{\mathbf{v}}$ being the unit wave vector. For the configuration shown in Fig. 2, every entry of **V** will have a form given by,

$$[\mathbf{V}]_{k,s}(\phi,\theta) = \exp\left(i2\pi\left((s-1)\frac{d_y}{\lambda}\sin\phi\sin\theta + (k-1)\frac{d_z}{\lambda}\cos\theta\right)\right), \tag{8}$$

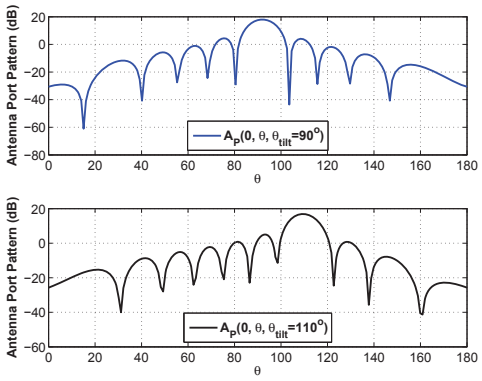

Fig. 3. Antenna port radiation pattern at different downtilt values.

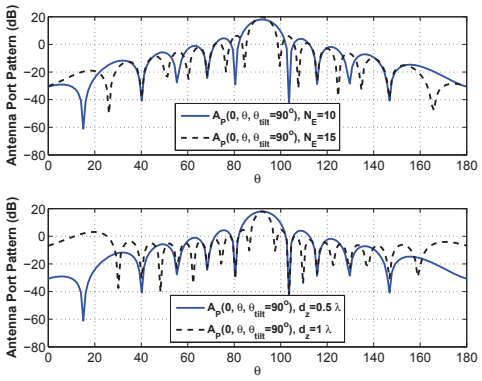

Fig. 4. Antenna port radiation pattern at different values of N_E and d_z.

where d_y is the horizontal separation between the antenna ports and d_z is the vertical separation between the antenna elements, with the phase reference at the origin.

Also $\mathbf{W}$ is a $N_E \times N_{BS}$ matrix comprising of the weights to be applied to the individual radiation elements, with each entry given by [7],

$$[\mathbf{W}]_{k,s}(\theta_{tilt_s}) = \frac{1}{\sqrt{N_E N_{BS}}} \exp\left(-i2\pi\left((s-1)\frac{d_y}{\lambda}\sin\phi_{scan}\sin\theta_{tilt_s} + (k-1)\frac{d_z}{\lambda}\cos\theta_{tilt_s}\right)\right), \tag{9}$$

where ϕ_{scan} is the horizontal steering angle and θ_{tilt_s} is the downtilt angle for the s^{th} port, defined between 0^o and 180^o. Denoting the $(k,s)^{th}$ entries of $\mathbf{W}$ and $\mathbf{V}$ as $w_s^k(\theta_{tilt_s})$ and $v_s^k(\phi,\theta)$ respectively, the small-scale 3D channel model constituted by the BS antenna port s is given by,

$$[\mathbf{h}]_s = \sum_{k=1}^{N_E} w_s^k(\theta_{tilt_s}) \sum_{n=1}^{N} \alpha_n \sqrt{g_E(\phi_n,\theta_n)} v_s^k(\phi_n,\theta_n), \tag{10}$$

$$= \mathbf{w}_s(\theta_{tilt_s})^T \sum_{n=1}^{N} \alpha_n \sqrt{g_E(\phi_n,\theta_n)} \mathbf{v}_s(\phi_n,\theta_n),\ s = 1,\ldots,N_{BS}, \tag{11}$$

where ϕ_n and θ_n are the azimuth and elevation angle of departure (AoD) of the n^{th} path respectively, and $\alpha_n \sim$ i.i.d $\mathcal{CN}(0,\frac{1}{N})$ is the amplitude of the n^{th} path. Also $\mathbf{w}_s(\theta_{tilt_s})$ is the weight vector for the s^{th} antenna port, given by the s^{th} column of $\mathbf{W}$, and $\mathbf{v}_s(\phi_n,\theta_n)$ is the s^{th} column of $\mathbf{V}$. The channel with a given antenna port is therefore a weighted sum of channels with the N_E elements inside it. This new representation is different from the 'antenna port approach' based models in [19], [13], where the channel is directly characterized between the ports.

The objective of the channel representation based on antenna elements is two fold: first, it allows for more flexibility in controlling the downtilt angle of every port since the channel is linearly dependent on the downtilt weights applied to the elements within it; second, it takes into account the pattern of side lobes in the antenna port radiation pattern, an effect which was discarded by the channel representation in ITU [19] and 3GPP TR36.814 [20]. This can be seen by plotting the antenna port radiation pattern $A_P(\phi, \theta, \theta_{tilt})$, which is computed as,

$$A_P(\phi, \theta, \theta_{tilt}) = A_E(\phi, \theta) + 20 \log_{10} |A_F(\theta, \theta_{tilt})|, \tag{12}$$

where $A_E(\phi, \theta)$ is given by (1) and $A_F(\theta, \theta_{tilt})$ is the array factor for the port given by,

$$A_F(\theta, \theta_{tilt}) = \sum_{k=1}^{N_E} w^k(\theta_{tilt}) \exp\left(i2\pi(k-1)\frac{d_z}{\lambda} \cos\theta \right). \tag{13}$$

We plot $A_P(\phi, \theta, \theta_{tilt})$ at $\phi = 0^o$ in Fig. 3 for $N_E = 10$, $d_z/\lambda = 0.5$, $G_{E,max} = 8\text{dBi}$ and $\phi_{3dB} = \theta_{3dB} = 65^o$. The weights are calculated using (9) for $\phi_{scan} = 0^o$, and $\theta_{tilt} = 90^o$ and 110^o. It can be seen that changing the weights shifts the main lobe of the radiation pattern to the desired value of downtilt angle. Fig. 4 studies the effect of N_E and d_z on the overall antenna port pattern. The first subplot confirms that increasing N_E results in a narrower main lobe of the radiation pattern, i.e. a smaller 3dB beamwidth. This enables more directed transmissions to the users. The second subplot shows that increasing d_z also achieves a smaller 3dB beamwidth.

III. Wavefield Decomposition and Spatial Correlation Function

The compact structure of the AAS and the small values of elevation angular spreads in realistic propagation environments cause the correlation between the antenna elements to dramatically increase, which makes it imperative to characterize and account for it when determining the performance gains realizable through FD-MIMO techniques. In this section, we derive a generalized analytical expression for the spatial correlation between antenna elements, considering realistic antenna patterns and arbitrary distributions of AoDs and AoAs. Some useful results on spherical harmonics are recalled first, which will be exploited later in the derivation.

A. Spherical Harmonic Expansion

In a 3D propagation environment, the array response of an antenna element can be expanded using the spherical decomposition of plane waves. Using the Jacobi-Anger expansion, a plane electromagnetic wave can be expanded as [28],

$$e^{ik\hat{\mathbf{v}}.\mathbf{x}} = \sum_{n=0}^{\infty} i^n (2n+1) j_n(k||\mathbf{x}||) P_n\left(\hat{\mathbf{v}}.\hat{\mathbf{x}}\right), \mathbf{x} \in \mathbb{R}^3, \tag{14}$$

where j_n is the n^{th} order spherical Bessel function, P_n is the n^{th} order Legendre polynomial function, $k = \frac{2\pi}{\lambda}$ is the wave number, $\hat{\mathbf{v}}$ is the unit vector in the direction of wave propagation and $\mathbf{x}$ is the location vector of the antenna element. Let (ϕ_1, θ_1) and (ϕ_2, θ_2) be the spherical coordinates of $\hat{\mathbf{v}}$ and $\hat{\mathbf{x}}$ respectively, then by the Legendre addition theorem,

$$P_n(\hat{\mathbf{v}}.\hat{\mathbf{x}}) = P_n(\cos\theta_1)P_n(\cos\theta_2) + 2\sum_{m=1}^{n}\frac{(n-m)!}{(n+m)!}P_n^m(\cos\theta_1)P_n^m(\cos\theta_2)\cos[m(\phi_1-\phi_2)], \quad (15)$$

where P_n^m are the associated Legendre polynomials.

B. Spatial Correlation Function for Antenna Elements

Using the antenna element radiation pattern and the array response expression of an individual element given in (8), and for $\alpha_n \sim i.i.d\, \mathcal{CN}(0, \frac{1}{N})$, the SCF for the channels constituted by (k, s) and (k', s') antenna elements in the AAS can be expressed as,

$$\begin{aligned}\rho_E(s-s', k-k') &= \mathbb{E}[h_{k,s}h^*_{k',s'}] = \mathbb{E}[g_E(\phi,\theta)v_s^k(\phi,\theta)v_{s'}^{k'*}(\phi,\theta)],\\ &= \mathbb{E}\left[g_E(\phi,\theta)\exp\left(i2\pi\left[\frac{d_y}{\lambda}(s-s')\sin\phi\sin\theta + \frac{d_z}{\lambda}(k-k')\cos\theta\right]\right)\right], \quad (16)\end{aligned}$$

where $k, k' = 1, \ldots, N_E$ and $s, s' = 1, \ldots, N_{BS}$. Let $Z_y = (s-s')\frac{d_y}{\lambda}$ and $Z_z = (k-k')\frac{d_z}{\lambda}$, and define $Z = \sqrt{Z_y^2 + Z_z^2}$ and,

$$\beta = \begin{cases} 0, & \text{if } s-s' = 0 \;\&\; k-k' = 0,\\ \arctan\left(\frac{Z_y}{Z_z}\right), & \text{if } s-s' > 0 \;\&\; k-k' \geq 0,\\ \pi + \arctan\left(\frac{Z_y}{Z_z}\right), & \text{if } s-s' \geq 0 \;\&\; k-k' < 0. \end{cases} \quad (17)$$

With these definitions and reformulations, (16) can be expressed as,

$$\rho_E(s-s', k-k') = \mathbb{E}\left[g_E(\phi,\theta)\exp\left(i2\pi Z\left[\cos\theta\cos\beta + \sin\theta\sin\beta\cos\left(\phi - \frac{\pi}{2}\right)\right]\right)\right], \quad (18)$$

for $(s-s' = 0 \;\&\; k-k' = 0)$, $(s-s' > 0 \;\&\; k-k' \geq 0)$ and $(s-s' \geq 0 \;\&\; k-k' < 0)$. Note that the other cases can be computed using $\rho_E(s-s', k-k') = \rho_E(s'-s, k'-k)^*$ for $(s-s' < 0 \;\&\; k-k' \leq 0)$, and $\rho_E(s-s', k-k') = \rho_E(s'-s, k'-k)^*$ for $(s-s' \leq 0 \;\&\; k-k' > 0)$.

Observe that $\cos\theta\cos\beta + \sin\theta\sin\beta\cos\left(\phi - \frac{\pi}{2}\right)$ is the dot product of $\hat{\mathbf{v}}(\phi,\theta)$ with $\hat{\mathbf{x}}(\pi/2, \beta)$, where $\mathbf{x}$ is the location vector between $(k, s)^{th}$ and $(k', s')^{th}$ elements. This representation allows us to expand (18) using (14) and (15) to yield,

$$\rho_E(s-s', k-k') = \mathbb{E}\Bigg[g_E(\phi,\theta)\sum_{n=0}^{\infty} i^n(2n+1)j_n(2\pi Z)\left(P_n(\cos\theta)P_n(\cos\beta) + 2\sum_{m=1}^{n}\frac{(n-m)!}{(n+m)!}\right.$$

$$\left.\times\, P_n^m(\cos\theta)P_n^m(\cos\beta)\cos\left(m\left(\phi - \frac{\pi}{2}\right)\right)\right)\Bigg]. \quad (19)$$

Next we systematically expand $\rho_E(s-s',k-k')$ by defining $\bar{P}_n^m(\mathrm{x})$=$\sqrt{(n+\frac{1}{2})\frac{(n-m)!}{(n+m)!}}P_n^m(\mathrm{x})$ and using the decomposition $g_E(\phi,\theta) \approx g_{E,H}(\phi)g_{E,V}(\theta)$ as,

$$\rho_E(s-s',k-k') = \mathbb{E}[g_E(\phi,\theta)]j_0\left(2\pi Z\right) + \sum_{n=1}^{\infty}(-1)^n(4n+1)j_{2n}\left(2\pi Z\right)P_{2n}(\cos\beta)\mathbb{E}[P_{2n}(\cos\theta)g_{E,V}(\theta)]$$
$$\times\,\mathbb{E}[g_{E,H}(\phi)] - \sum_{n=1}^{\infty} i(-1)^n(4n-1)j_{2n-1}\left(2\pi Z\right)P_{2n-1}(\cos\beta)\mathbb{E}[P_{2n-1}(\cos\theta)g_{E,V}(\theta)]\mathbb{E}[g_{E,H}(\phi)]$$
$$+\sum_{n=1}^{\infty}4(-1)^n j_{2n}\left(2\pi Z\right)\Bigg(\Bigg(\sum_{m=1}^{n}(-1)^m\bar{P}_{2n}^{2m}(\cos\beta)\mathbb{E}[\bar{P}_{2n}^{2m}(\cos\theta)g_{E,V}(\theta)]\mathbb{E}[\cos(2m\phi)g_{E,H}(\phi)]\Bigg)$$
$$-\left(\sum_{m=1}^{n}(-1)^m\bar{P}_{2n}^{2m-1}(\cos\beta)\mathbb{E}[\bar{P}_{2n}^{2m-1}(\cos\theta)g_{E,V}(\theta)]\mathbb{E}[\sin((2m-1)\phi)g_{E,H}(\phi)]\right)\Bigg) + \sum_{n=1}^{\infty}4i(-1)^n$$
$$\times\, j_{2n-1}\left(2\pi Z\right)\Bigg(\Bigg(\sum_{m=1}^{n}(-1)^m\bar{P}_{2n-1}^{2m-1}(\cos\beta)\mathbb{E}[\bar{P}_{2n-1}^{2m-1}(\cos\theta)g_{E,V}(\theta)]\mathbb{E}[\sin((2m-1)\phi)g_{E,H}(\phi)]\Bigg)$$
$$-\left(\sum_{m=1}^{n}(-1)^m\bar{P}_{2n-1}^{2m}(\cos\beta)\mathbb{E}[\bar{P}_{2n-1}^{2m}(\cos\theta)g_{E,V}(\theta)]\mathbb{E}[\cos(2m\phi)g_{E,H}(\phi)]\right)\Bigg). \tag{20}$$

The random variables, AoDs, appear as arguments of Legendre polynomials in (20) and it is important to have a general representation for these polynomials to facilitate the development of the expectation terms in a closed-form. For this purpose, we use the trigonometric expansion of Legendre polynomials from [29]. The following Lemma expresses the Legendre and associated Legendre polynomials with even and odd orders as a linear combination of sines and cosines.

Lemma 1. For non-negative integers n and m,

$$\begin{aligned}
P_{2n}(\cos x) &= p_n^2 + 2\sum_{k=1}^{n} p_{n-k}p_{n+k}\cos(2kx),\\
P_{2n-1}(\cos x) &= 2\sum_{k=1}^{n} p_{n-k}p_{n+k-1}\cos((2k-1)x),\\
\bar{P}_{2n}^{2m}(\cos x) &= \sum_{k=0}^{n} c_{2n,2k}^{2m}\cos(2kx),\\
\bar{P}_{2n}^{2m-1}(\cos x) &= \sum_{k=1}^{n} d_{2n,2k}^{2m-1}\sin(2kx),\\
\bar{P}_{2n-1}^{2m}(\cos x) &= \sum_{k=1}^{n} c_{2n-1,2k-1}^{2m}\cos((2k-1)x),\\
\bar{P}_{2n-1}^{2m-1}(\cos x) &= \sum_{k=1}^{n} d_{2n-1,2k-1}^{2m-1}\sin((2k-1)x),
\end{aligned} \tag{21}$$

where $p_n, c^{2m}_{2n,2k}, c^{2m}_{2n-1,2k-1}, d^{2m-1}_{2n,2k}$ and $d^{2m-1}_{2n-1,2k-1}$ are given by the recursion relations in [29].

Using a similar development as done in [30], these trigonometric expansions will be shown to express $\rho_E(s-s', k-k')$ in terms of the FS coefficients of the PAS and PES defined as [31],

$$\text{PAS}_E(\phi) = g_{E,H}(\phi)p_\phi(\phi), \tag{22}$$

$$\text{PES}_E(\theta) = g_{E,V}(\theta)p_\theta(\theta), \tag{23}$$

where the angular power density functions, $p_\phi(\phi)$=$f_\phi(\phi)$ and $p_\theta(\theta)$=$\frac{f_\theta(\theta)}{\sin(\theta)}$, with $f_\phi(\phi)$ and $f_\theta(\theta)$ being the probability density functions of the azimuth and elevation angles respectively.

The FS coefficients, $a_\phi(m), b_\phi(m), a_\theta(k)$ and $b_\theta(k)$, for the PAS and PES are defined as,

$$a_\phi(m) = \frac{1}{\pi}\int_{-\pi}^{\pi} \text{PAS}_E(\phi)\cos(m\phi)d\phi, \tag{24}$$

$$b_\phi(m) = \frac{1}{\pi}\int_{-\pi}^{\pi} \text{PAS}_E(\phi)\sin(m\phi)d\phi, \tag{25}$$

$$a_\theta(k) = \frac{1}{\pi}\int_{0}^{\pi} \text{PES}_E(\theta)\cos(k\theta)d\theta, \tag{26}$$

$$b_\theta(k) = \frac{1}{\pi}\int_{0}^{\pi} \text{PES}_E(\theta)\sin(k\theta)d\theta. \tag{27}$$

Exploiting **Lemma 1**, the expectation terms in (20) are expressed analytically as a linear combination of the FS coefficients of PAS and PES, resulting in **Theorem 1**.

Theorem 1. For an AAS with a 2D uniform planar array of antenna elements with arbitrary antenna patterns and for arbitrary angular distributions, such that $\phi \in [-\pi, \pi]$ and $\theta \in [0, \pi]$, the 3D SCF for the channels constituted by (k, s) and (k', s') antenna elements is given by,

$$\rho_E(s-s', k-k') = \pi^2 a_\phi(0)b_\theta(1)j_0\left(2\pi Z\right) + \sum_{n=1}^{\infty}(-1)^n(4n+1)j_{2n}\left(2\pi Z\right)P_{2n}(\cos\beta)\pi^2 \tag{28}$$

$$\times\, a_\phi(0)\sum_{k=-n}^{n} p_{n-k}p_{n+k}\frac{1}{2}[b_\theta(2k+1) - b_\theta(2k-1)] - \sum_{n=1}^{\infty} i(-1)^n(4n-1)j_{2n-1}\left(2\pi Z\right)P_{2n-1}(\cos\beta)a_\phi(0)\pi^2$$

$$\times\, 2\sum_{k=1}^{n} p_{n-k}p_{n+k-1}\frac{1}{2}[b_\theta(2k) - b_\theta(2k-2)] + \sum_{n=1}^{\infty} 4(-1)^n j_{2n}\left(2\pi Z\right)\Bigg[\Bigg(\sum_{m=1}^{n}(-1)^m \bar{P}^{2m}_{2n}(\cos\beta)a_\phi(2m)\frac{\pi^2}{2}$$

$$\times \sum_{k=0}^{n} c^{2m}_{2n,2k}[b_\theta(2k+1) - b_\theta(2k-1)]\Bigg) - \Bigg(\sum_{m=1}^{n}(-1)^m \bar{P}^{2m-1}_{2n}(\cos\beta)b_\phi(2m-1)\frac{\pi^2}{2}\sum_{k=1}^{n} d^{2m-1}_{2n,2k}[a_\theta(2k-1)$$

$$- a_\theta(2k+1)]\Bigg)\Bigg] + \sum_{n=1}^{\infty} 4i(-1)^n j_{2n-1}\left(2\pi Z\right)\Bigg[\Bigg(\sum_{m=1}^{n}(-1)^m \bar{P}^{2m-1}_{2n-1}(\cos\beta)b_\phi(2m-1)\frac{\pi^2}{2}\sum_{k=1}^{n} d^{2m-1}_{2n-1,2k-1}$$

$$\times\, [a_\theta(2k-2) - a_\theta(2k)]\Bigg) - \Bigg(\sum_{m=1}^{n}(-1)^m \bar{P}^{2m}_{2n-1}(\cos\beta)a_\phi(2m)\frac{\pi^2}{2}\sum_{k=1}^{n} c^{2m}_{2n-1,2k-1}[b_\theta(2k) - b_\theta(2k-2)]\Bigg)\Bigg],$$

for ($s-s'=0$ & $k-k'=0$), ($s-s'>0$ & $k-k'\geq 0$) and ($s-s'\geq 0$ & $k-k'<0$). For other cases, $\rho_E(s-s',k-k')$ is computed as $\rho_E(s-s',k-k')=\rho_E(s'-s,k'-k)^*$ for ($s-s'<0$ & $k-k'\leq 0$), and $\rho_E(s-s',k-k')=\rho_E(s'-s,k'-k)^*$ for ($s-s'\leq 0$ & $k-k'>0$).

Using the analysis in [30], the summations over n can be truncated to $N_0=10$ terms, such that the truncation error in the correlation between adjacent elements ($.5\lambda$ spacing) in the AAS is bounded by $\sim 0.5\%$. This is the first explicit derivation of the SCF for antenna elements constituting the 2D AAS. In contrast to the previous works on spatial correlation [23]–[25], the proposed generalized method does not assume any particular form for the underlying patterns and angular distributions. The researchers and industrials interested in using this model just need to provide the FS coefficients of the PAS and PES for any propagation environment under study.

C. Spatial Correlation Function for Antenna Ports

In FD-MIMO techniques, the radio resource is organized on the basis of antenna ports, where each port is used to transmit a data symbol at a particular value of the downtilt angle, θ_{tilt}. It is therefore important to characterize the correlation between the overall antenna ports.

From (10) it is evident that the SCF for the channels constituted by any two antenna ports, s and s', will be a function of the correlations between all the elements constituting these ports and the weight functions applied to these elements as,

$$\rho(s,s')=\mathbb{E}[[\mathbf{h}]_s[\mathbf{h}]_{s'}^H]=\sum_{k=1}^{N_E}\sum_{k'=1}^{N_E} w_s^k(\theta_{tilt_s})w_{s'}^{k'*}(\theta_{tilt_{s'}})\mathbb{E}[g_E(\phi,\theta)v_s^k(\phi,\theta)v_{s'}^{k'*}(\phi,\theta)],$$

$$=\sum_{k=1}^{N_E}\sum_{k'=1}^{N_E} w_s^k(\theta_{tilt_s})w_{s'}^{k'*}(\theta_{tilt_{s'}})\rho_E(s-s',k-k'),\ \text{for } s,s'=1,\ldots,N_{BS}, \tag{29}$$

where $\rho_E(s-s',k-k')$ is given by (28). The $N_{BS}\times N_{BS}$ correlation matrix for the antenna ports constituting the AAS can therefore be written as,

$$\mathbf{R}^{BS}=\widetilde{\mathbf{W}}^H\mathbf{R}^E\widetilde{\mathbf{W}}, \tag{30}$$

where $\widetilde{\mathbf{W}}$ is a $N_{BS}N_E\times N_{BS}$ block diagonal matrix of the weight vectors applied to the N_{BS} antenna ports given by,

$$\widetilde{\mathbf{W}}^H=\begin{bmatrix} \mathbf{w}_1{}^H & \mathbf{0}^{1\times N_E} & \mathbf{0}^{1\times N_E(N_{BS}-2)} \\ \mathbf{0}^{1\times N_E} & \mathbf{w}_2{}^H & \mathbf{0}^{1\times N_E(N_{BS}-2)} \\ & & \ddots \\ \mathbf{0}^{1\times N_E} & \mathbf{0}^{1\times N_E(N_{BS}-2)} & \mathbf{w}_{N_{BS}}{}^H \end{bmatrix}, \tag{31}$$

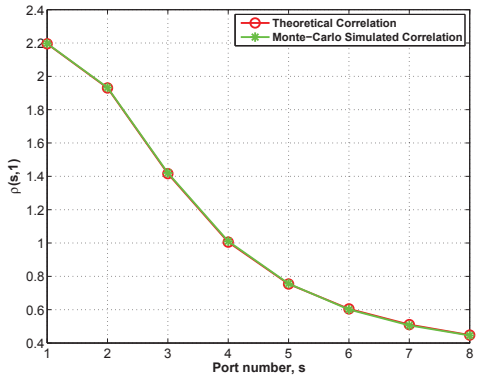

Fig. 5. Validation of the proposed SCF.

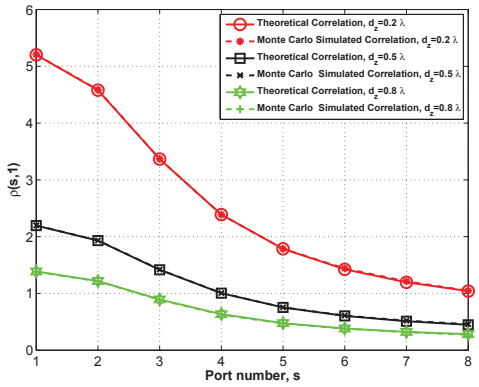

Fig. 6. Effect of d_z on correlation.

where $\mathbf{w}_s$ as defined in (11) is the $N_E \times 1$ weight vector for the s^{th} antenna port given by the s^{th} column of the weight matrix $\mathbf{W}$ in (9), i.e. $\mathbf{w}_s = \mathbf{W}(:, s)$ and $\mathbf{R}^E$ is the $N_{BS}N_E \times N_{BS}N_E$ correlation matrix for all the elements constituting the AAS defined as,

$$[\mathbf{R}^E]_{(s'-1)N_E+k',(s-1)N_E+k} = \rho_E(s-s', k-k'), \quad k, k' = 1, \ldots, N_E, \quad s, s' = 1, \ldots, N_{BS}, \quad (32)$$

where $\rho_E(s-s', k-k')$ is given by (28). With this formulation, $[\mathbf{R}_{BS}]_{s',s} = \rho(s, s')$.

In order to validate the proposed SCF, all antenna ports are assumed to transmit at a downtilt angle of $\theta_{tilt_s} = 90^o$, $s = 1, \ldots, N_{BS}$. The elevation angles are generated according to Laplacian density spectrum, with mean AoD θ_0 and spread σ_t. The azimuth angles are generated using VM distribution, with mean μ and a measure of spread, κ_t. The parameter values are set as $N_0 = 30$, $\sigma_t = 15^o$, $\theta_0 = 100^o$, $\kappa_t = 10$ and $\mu = \pi/3$. The validation of the theoretical result in (29), where $\rho_E(s-s', k-k')$ is computed using (28), is done by comparison with the Monte-Carlo simulated correlation. The Monte Carlo simulations are performed over 100000 realizations of (16) to obtain the simulated $\rho_E(s-s', k-k')$. The correlation values are computed for antenna port s, $s = 1, \ldots, N_{BS}$, with reference to port 1. The results are shown in Fig. 5 for $N_E = 10$, $N_{BS} = 8$ and $d_y = d_z = 0.5\lambda$ [6]. The derived theoretical result provides a perfect fit to the Monte Carlo simulated correlation for only 30 summations over n, with the correlation values decreasing as the distance between the port pair increases. In Fig. 6, the effect of increasing d_z is shown to decrease the correlation between the antenna ports. The reason is attributed to the fact that for higher d_z, the main lobe of the radiation pattern as shown in Fig. 4 is narrower and as a consequence, the energy of many propagation paths, particularly at high angular spreads, is not captured by the antenna pattern, resulting in a decrease in Tx power and correlation.

IV. Performance Optimization of FD-MIMO Systems

The previous section expressed the spatial correlation between the antenna ports as a function of the correlation between the elements constituting the ports and the downtilt weights applied to these elements. In this section, we optimize these weight vectors to maximize the downlink SNR and SIR in the single user and multi-user MISO settings respectively. Existing works on 3D beamforming use the ITU approach to model the vertical dimension of the antenna port radiation pattern in an approximate fashion, ignoring the dependency of the pattern on the construction of the port, i.e. the values of N_E, d_z, and the downtilt weights [14], [21], [22]. This work aims to make one of the preliminary contributions in this area by formulating and proposing solutions for the downtilt weight optimization problem, utilizing a correlation based channel model.

It is important for channel models to take the spatial correlation between antenna elements into account to allow for a more accurate performance analysis of elevation beamforming techniques. The parametric channel model discussed in Section II-B is one way to generate correlated FD-MIMO channels. However, optimizing the downtilt weights dynamically using this model would require the acquisition of high-dimension instantaneous channel state information (CSI). The explicit dependence of the channel on the number of paths and associated small-scale parameters (AoDs, AoAs, powers) makes the analysis intractable. We propose to use the developed SCF in **Theorem 1** to form the non-parametric Kronecker channel model instead, which is defined as,

$$\mathbf{H} = \mathbf{R}_{MS}^{\frac{1}{2}} \mathbf{X} \mathbf{R}_{BS}^{\frac{1}{2}}, \tag{33}$$

where $\mathbf{X}$ is a N_{MS}xN_{BS} matrix with $\mathcal{CN}$(0,1) entries, and $\mathbf{R}_{MS}$ and $\mathbf{R}_{BS}$ are the correlation matrices at the MS and the BS respectively. This model will not only allow us to exploit tools from random matrix theory (RMT) to propose solutions for the optimal downtilt weight vectors, but will also release the high dependence on the instantaneous CSI by allowing us to utilize the quasi-static channel correlation matrices of the users to learn the optimal weights. The computation of these matrices using the derived SCF in the last section requires knowledge of the large-scale parameters only (mean AoDs/AoAs and angular spreads at the BS and the MS).

In this section, the focus is on FD-MISO settings, with the non-parametric channel model for a single antenna user served by a BS equipped with a $N_E \times N_{BS}$ AAS given as follows.

Assumption A-1. *The channel vector, $\boldsymbol{h} \in \mathbb{C}^{N_{BS} \times 1}$, for a user equipped with a single omnidirectional Rx antenna element is modeled as [32],*

$$\mathbf{h} = \mathbf{R}_{BS}^{\frac{1}{2}} \mathbf{z}, \tag{34}$$

where $\boldsymbol{z}$ *has i.i.d zero mean, unit variance complex Gaussian entries and* $\boldsymbol{R}_{BS}$ *is the user's channel covariance matrix given by* $\boldsymbol{R}_{BS} = \widetilde{\boldsymbol{W}}^H \boldsymbol{R}^E \widetilde{\boldsymbol{W}}$*, where* $\widetilde{\boldsymbol{W}}$ *and* $\boldsymbol{R}^E$ *are defined in (31) and (32) respectively. The channel covariance matrix satisfies the condition,*

$$\limsup_{N_{BS}} ||\boldsymbol{R}_{BS}|| < +\infty. \tag{35}$$

Before formulating the optimization problems for the downtilt weight vectors, we shall recall an important trace lemma that plays a key role in the problem formulations and analysis.

Lemma 2 ([33] Lemma 14.2). Let $\mathbf{A} \in \mathbb{C}^{N \times N}$ and $\mathbf{x} = [x_1, \ldots, x_N]^T \in \mathbb{C}^{N \times 1}$ be a random vector of i.i.d. entries independent of $\mathbf{A}$, such that $\mathbb{E}[x_i] = 0$, $\mathbb{E}[|x_i|^2] = 1$, $\mathbb{E}[|x_i|^8] < \infty$, and $\limsup_N ||\mathbf{A}|| < \infty$. Then,

$$\frac{1}{N}\mathbf{x}^H \mathbf{A}\mathbf{x} - \frac{1}{N} tr\ \mathbf{A} \xrightarrow[N \to \infty]{a.s.} 0. \tag{36}$$

A. Elevation Beamforming in a Single-User MISO System

The downlink of a single-cell MISO system is considered first, where a $N_E \times N_{BS}$ AAS at the BS serves a single user equipped with a single antenna element. The received complex baseband signal y at the user is given by,

$$y = \sqrt{\varrho}\mathbf{h}^H \mathbf{x} + n, \tag{37}$$

where $\mathbf{x} \in \mathbb{C}^{N_{BS} \times 1}$ is the Tx signal from the AAS, $\mathbf{h}^H \in \mathbb{C}^{1 \times N_{BS}}$ is the channel vector from the BS to the user given by (34) and $n \sim \mathcal{CN}(0, \sigma_n^2)$ is the additive white Gaussian noise (AWGN) with variance σ_n^2 at the user. Also ϱ is given by,

$$\varrho = P_{Tx} \times \text{PL} \times \text{SF} \times 10^{\frac{G_{E,max}}{10}}, \tag{38}$$

where PL is the path loss experienced by the user, SF is the shadow fading and P_{Tx} is the transmitted power. The downlink SNR for the user is then given by,

$$\gamma = \frac{\varrho}{\sigma_n^2} tr(\mathbf{h}\mathbf{h}^H). \tag{39}$$

We are interested in finding the SNR maximizing $N_E \times 1$ weight vectors $\mathbf{w}_s$, $s = 1, \ldots, N_{BS}$, that form the $\widetilde{\mathbf{W}}$ matrix defined in (31). The optimization problem is formulated as follows:

Problem (P1):

$$\underset{\mathbf{w}_1, \mathbf{w}_2, \ldots, \mathbf{w}_{N_{BS}}}{\text{maximize}}\ \gamma \tag{40}$$

$$\text{subject to } ||\mathbf{w}_s||_2 = 1, \text{ for } s = 1, \ldots, N_{BS}. \tag{41}$$

The constraint in (41) ensures that the total power of every antenna port is bounded and does not grow indefinitely with the number of elements stacked in a port. This problem has a simple solution in the large (N_{BS}, N_E) regime given in the following theorem.

Theorem 2. Consider a single user system consisting of a BS equipped with a $N_E \times N_{BS}$ AAS serving a single-antenna user, having the channel covariance matrix $\mathbf{R}_{BS}$. Then in the large (N_{BS}, N_E) regime, the optimal 3D beamforming weight vectors $\mathbf{w}_s^*$ can be computed as,

$$\mathbf{w}_s^* = \mathbf{v}_{\lambda_{max}(\mathbf{R}_{ss}^E)}, \qquad s = 1, \ldots, N_{BS}, \tag{42}$$

where $\mathbf{v}_{\lambda_{max}(\mathbf{R}_{ss}^E)}$ is the eigenvector corresponding to the maximum eigenvalue λ_{max} of $\mathbf{R}_{ss}^E$, where $\mathbf{R}_{ss}^E$ is a $N_E \times N_E$ matrix given by $\mathbf{R}^E([(s-1)N_E + 1 : sN_E], [(s-1)N_E + 1 : sN_E])$, for $\mathbf{R}^E$ defined in (32), such that,

$$\mathbf{R}_{ss}^{E\,\frac{1}{2}} \mathbf{w}_s^* = \sqrt{\lambda_{max}(\mathbf{R}_{ss}^E)} \mathbf{w}_s^*. \tag{43}$$

Physically, $\mathbf{R}_{ss}^E$ is the correlation matrix formed by the elements of port s and is therefore given by the s^{th} $N_E \times N_E$ diagonal matrix of $\mathbf{R}^E$. The proof is postponed to Appendix A.

B. 3D Beamforming in a Multi-User MISO System

The downlink of a multi-user MISO system is considered next, where a $N_E \times N_{BS}$ AAS serves K non-cooperating single-element users. The BS uses linear precoding in the digital domain to mitigate inter-user interference. The precoding vector and the data symbol for the k^{th} user are denoted by $\mathbf{g}_k \in \mathbb{C}^{N_{BS} \times 1}$ and $s_k \sim \mathcal{CN}(0, 1)$ respectively. The BS transmits the $N_{BS} \times 1$ signal:

$$\mathbf{x} = \sum_{k=1}^{K} \mathbf{g}_k s_k = \mathbf{G}\mathbf{s}, \tag{44}$$

where $\mathbf{G}$ is the $N_{BS} \times K$ precoding matrix and $\mathbf{s}$ is the $K \times 1$ vector of data symbols. The received complex baseband signal at the user k, y_k, is given by,

$$y_k = \sum_{l=1}^{K} \sqrt{\varrho_k} \mathbf{h}_k^H \mathbf{g}_l s_l + n_k, \tag{45}$$

where $\mathbf{h}_k^H \in \mathbb{C}^{1 \times N_{BS}}$ is the channel vector from the BS to the user k defined in (34) as $\mathbf{h}_k = \mathbf{R}_{BS_k}^{\frac{1}{2}} \mathbf{z}_k$, where the condition described in **Assumption A-1** on the channel convariance matrices holds. Every per user channel covariance matrix $\mathbf{R}_{BSk}$ is given by $\mathbf{R}_{BSk} = \widetilde{\mathbf{W}}^H \mathbf{R}_k^E \widetilde{\mathbf{W}}$ as defined in (30), where $\widetilde{\mathbf{W}}$ and $\mathbf{R}_k^E$ are defined in (31) and (32) respectively. Also $n_k \sim \mathcal{CN}(0, \sigma_n^2)$ is the AWGN with variance σ_n^2 at the user k and ϱ_k is computed using (38) for each user.

Linear precoding schemes are generally asymptotically optimal in the large (N_{BS}, K) regime [2] and robust to CSI imperfections [3]. However, the complexity of computing these state-of-the-art linear precoding schemes is prohibitively high in the large (N_{BS}, K) regime. A notable exception is the matched filter (MF), also known as maximum ratio transmission (MRT) [34], which is a popular scheme for large scale MIMO systems due to its low computational complexity, robustness, and high asymptotic performance [2]. Therefore, we focus on the MF precoding given by the conjugate of the channel vector $\mathbf{h}_k^H$ as,

$$g_k = \beta \mathbf{h}_k, \tag{46}$$

where β is chosen to satisfy the Tx power constraint $tr(\mathbf{G}\mathbf{G}^H) = 1$ and turns out to be,

$$\beta = \frac{1}{\sqrt{tr(\mathbf{H}\mathbf{H}^H)}}, \tag{47}$$

where $\mathbf{H} = [\mathbf{h}_1 \mathbf{h}_2 \dots \mathbf{h}_K]$.

1) Problem Formulation: The focus of this section is on interference limited systems, so the performance metric employed is the SIR defined for user k as,

$$SIR_k = \frac{\mathbf{h}_k^H \mathbf{g}_k \mathbf{g}_k^H \mathbf{h}_k}{\sum_{l \neq k}^{K} \mathbf{h}_k^H \mathbf{g}_l \mathbf{g}_l^H \mathbf{h}_k}. \tag{48}$$

The SIR for the MF precoding can be re-written as,

$$SIR_k = \frac{|\mathbf{h}_k^H \mathbf{h}_k|^2}{\sum_{l \neq k}^{K} \mathbf{h}_k^H \mathbf{h}_l \mathbf{h}_l^H \mathbf{h}_k}, \tag{49}$$

An asymptotic analysis of this quantity would yield a deterministic approximation for the SIR in the large (N_{BS}, N_E) regime as stated in the following proposition.

Proposition 1. Consider a multi-user MISO system consisting of a BS equipped with a $N_E \times N_{BS}$ active antenna array system serving K non co-operating single antenna users, having channel covariance matrices $\mathbf{R}_{BSk}$, $k = 1, \dots, K$ that satisfy the condition in **Assumption A-1**. Then in the large (N_{BS}, N_E) regime,

$$SIR_k - \frac{\frac{1}{N_{BS}^2}(\ tr\mathbf{R}_{BSk})^2}{\frac{1}{N_{BS}^2}\sum_{l \neq k}^{K} tr(\mathbf{R}_{BSk}\mathbf{R}_{BSl})} \xrightarrow{a.s.} 0, \quad k = 1, \dots, K. \tag{50}$$

The proof of **Proposition 1** is provided in Appendix B. Now given that $\mathbf{R}_{BS,k} = \widetilde{\mathbf{W}}^H \mathbf{R}_k^E \widetilde{\mathbf{W}}$ as defined in (30), (31), and (32), the SIR converges in the large (N_{BS}, N_E) to the following,

$$SIR_k - \frac{(\frac{1}{N_{BS}}\sum_{s=1}^{N_{BS}} \mathbf{w}_s^H \mathbf{R}_{k,ss}^E \mathbf{w}_s)^2}{\frac{1}{N_{BS}^2}\sum_{l \neq k}^{K}\sum_{s,s'=1}^{N_{BS}} \mathbf{w}_s^H \mathbf{R}_{k,ss'}^E \mathbf{w}_{s'} \mathbf{w}_{s'}^H \mathbf{R}_{l,s's}^E \mathbf{w}_s} \xrightarrow{a.s.} 0, \tag{51}$$

where $\mathbf{w}_s$ and $\mathbf{w}_{s'}$ are the $N_E \times 1$ weight vectors for the antenna ports s and s' forming the block diagonal matrix $\widetilde{\mathbf{W}}$ in (31). $\mathbf{R}^E_{k,ss}$ is a $N_E \times N_E$ matrix given by $\mathbf{R}^E_k([(s-1)N_E+1 : sN_E], [(s-1)N_E+1 : sN_E])$, where $\mathbf{R}^E_k$ is defined in (32) and is computed for user k, $k = 1, \ldots, K$. Similarly $\mathbf{R}^E_{k,ss'}$ is a $N_E \times N_E$ matrix given by $\mathbf{R}^E_k([(s-1)N_E+1 : sN_E], [(s'-1)N_E+1 : s'N_E])$.

$\mathbf{R}^E_{k,ss}$ refers to the correlation matrix formed by the elements of port s, given by the s^{th} $N_E \times N_E$ block diagonal matrix of $\mathbf{R}^E_k$ and $\mathbf{R}^E_{k,ss'}$ refers to the cross-correlation matrix between the elements of port s and port s', given by the (s^{th}, s'^{th}) $N_E \times N_E$ block matrix of $\mathbf{R}^E_k$.

The performance metric in this section is the max min SIR, which provides a good balance between system throughput, user fairness, and computational complexity. Using the deterministic equivalent just worked out, the optimization problem is formulated as,

Problem (P2):

$$\underset{\mathbf{w}_1, \mathbf{w}_2, \ldots \mathbf{w}_{N_{BS}}}{\text{maximize}} \; \underset{k \in \{1,\ldots,K\}}{\text{minimize}} \quad \frac{(\sum_{s=1}^{N_{BS}} \mathbf{w}_s^H \mathbf{R}^E_{k,ss} \mathbf{w}_s)^2}{\sum_{l \neq k}^{K} \sum_{s,s'=1}^{N_{BS}} \mathbf{w}_s^H \mathbf{R}^E_{k,ss'} \mathbf{w}_{s'} \mathbf{w}_{s'}^H \mathbf{R}^E_{l,s's} \mathbf{w}_s} \tag{52}$$

$$\text{subject to} \quad ||\mathbf{w}_s||_2 = 1, \quad s \in \{1, \ldots, N_{BS}\}. \tag{53}$$

The problem of optimizing the beamforming weights through joint max-min problem formulations has been considered in [35], where the problem of multi-cast beamforming with different receiver groups was shown to be NP-hard (see Claim 2 in [35]) and was solved quasi-optimally using semi-definite relaxation (SDR). The problem at hand is much harder because it considers the joint optimization of different weight vectors for different antenna ports. Even after applying SDR and substituting the positive semi-definite rank-one matrix $\mathbf{w}_s \mathbf{w}_s^H \in \mathbb{C}^{N_E \times N_E}$ for a positive semi-definite matrix $\mathbf{W}_s \in \mathbb{C}^{N_E \times N_E}$ of arbitrary rank, the relaxed problem is not tractable because of the product of $\mathbf{W}_s$ and $\mathbf{W}_{s'}$ in the denominator of the objective function. In order to enable a tractable relaxation, all the antenna ports are assumed to transmit using the same optimal downtilt weight vector. Dropping the subscripts s and s', the resulting problem is given as,

Problem (P3):

$$\underset{\mathbf{w}}{\text{maximize}} \; \underset{k \in \{1,\ldots,K\}}{\text{minimize}} \quad \frac{(\sum_{s=1}^{N_{BS}} tr(\mathbf{w}\mathbf{w}^H \mathbf{R}^E_{k,ss}))^2}{\sum_{l \neq k}^{K} \sum_{s,s'=1}^{N_{BS}} tr(\mathbf{w}\mathbf{w}^H \mathbf{R}^E_{k,ss'} \mathbf{w}\mathbf{w}^H \mathbf{R}^E_{l,s's})} \tag{54}$$

$$\text{subject to} \quad tr(\mathbf{w}\mathbf{w}^H) = 1. \tag{55}$$

This is a basic elevation beamforming scenario referred to as single downtilt beamforming. However, the problem of optimization of the weight vectors for the exact 3GPP TR36.873 3D channel model has not been addressed in a previous work so it is useful to lay the groundwork

and see the extent of performance gains realizable. In the next section, we will deal with the more complicated case of different weight vectors for different antenna ports. Now substituting the positive semi-definite rank-one matrix $\mathbf{w}\mathbf{w}^H \in \mathbb{C}^{N_E \times N_E}$ in *Problem (P3)* for a positive semi-definite matrix $\mathbf{W} \in \mathbb{C}^{N_E \times N_E}$ of arbitrary rank, the semi-definite relaxed problem is given as,

Problem (P4):

$$\underset{\mathbf{W}}{\text{maximize}} \quad \underset{k\in\{1,\ldots,K\}}{\text{minimize}} \qquad \frac{(\sum_{s=1}^{N_{BS}} tr(\mathbf{W}\mathbf{R}_{k,ss}^{E}))^2}{\sum_{l\neq k}^{K}\sum_{s,s'=1}^{N_{BS}} tr(\mathbf{W}\mathbf{R}_{k,ss'}^{E}\mathbf{W}\mathbf{R}_{l,s's}^{E})} \tag{56}$$

$$\text{subject to} \qquad \mathbf{W} \succeq 0, tr(\mathbf{W}) = 1. \tag{57}$$

Problem (P4) is efficiently solved using fractional programmings tools as discussed now.

2) Optimization Technique and Solution: Fractional programming provides efficient tools to maximize the minimum of ratios in which the numerator is a concave function, the denominator is a convex function, and the constraint set is convex, whereas no low-complexity optimization method is available if any of these properties is not met [36], [37] . An efficient method to do so is the generalized Dinkelbach's algorithm, discussed in Appendix A of [37]. In order to meet the conditions for application of Dinkelbach's method, *Problem (P4)* is reformulated as,

Problem (P5):

$$\underset{\mathbf{W}}{\text{maximize}} \quad \underset{k\in\{1,\ldots,K\}}{\text{minimize}} \qquad \frac{\sum_{s=1}^{N_{BS}} tr(\mathbf{W}\mathbf{R}_{k,ss}^{E})}{\sqrt{\sum_{l\neq k}^{K}\sum_{s,s'=1}^{N_{BS}} tr(\mathbf{W}\mathbf{R}_{k,ss'}^{E}\mathbf{W}\mathbf{R}_{l,s's}^{E})}} \tag{58}$$

$$\text{subject to} \qquad \mathbf{W} \succeq 0, tr(\mathbf{W}) = 1. \tag{59}$$

The objective function in (58) considers a set of ratios of two functions, where we denote the numerator by $f_k(\mathbf{W})$ and the denominator by $g_k(\mathbf{W})$, $k = 1, \ldots, K$. In order to study these functions, the following properties of the vec function are exploited.

Lemma 3: For any matrix $\mathbf{A} \in \mathbb{C}^{M\times N}$, the vec operator is defined as [38],

$$vec(\mathbf{A}) = (a_{11}, \ldots, a_{M1}, a_{12}, \ldots, a_{M2}, \ldots, a_{1N}, \ldots, a_{MN})^T. \tag{60}$$

Some properties of the vec operator are:

$$tr(\mathbf{AB}) = vec(\mathbf{A}^T)^T vec(\mathbf{B}), \quad \forall \mathbf{A}, \mathbf{B} \in \mathbb{C}^{M\times M}, \tag{61}$$

$$tr(\mathbf{A}^T\mathbf{BCD}^T) = vec(\mathbf{A})^T(\mathbf{D}\otimes\mathbf{B})vec(\mathbf{C}), \quad \forall \mathbf{A}, \mathbf{B}, \mathbf{C}, \mathbf{D} \in \mathbb{C}^{M\times M} \tag{62}$$

Exploiting these properties, $f_k(\mathbf{W})$ and $g_k(\mathbf{W})$ can be expressed as,

$$f_k(\mathbf{W}) = \sum_{s=1}^{N_{BS}} vec(\mathbf{W}^T)^T vec(\mathbf{R}_{k,ss}^{E}). \tag{63}$$

Algorithm 1 Optimization of Elevation Beamforming Vector

procedure GENERALIZED DINKELBACH($\mathbf{W}$)
  Set $\epsilon > 0$;
  Initialize $\lambda = 0$;
  repeat
    $\mathbf{W}^* = \max_{\mathbf{W} \in \mathbb{C}^{N_E \times N_E}} \{ \min_{1 \leq k \leq K} [f_k(\mathbf{W}) - \lambda g_k(\mathbf{W})] \}$, where $f_k(\mathbf{W})$ and $g_k(\mathbf{W})$ are given by (63) and (65) respectively, subject to $\mathbf{W} \succeq 0$ and $tr(\mathbf{W}) = 1$;
    $F = \min_{1 \leq k \leq K} \{ f_k(\mathbf{W}^*) - \lambda g_k(\mathbf{W}^*) \}$;
    $\lambda = \min_{1 \leq k \leq K} f_k(\mathbf{W}^*) / g_k(\mathbf{W}^*)$;
  until $F < \epsilon$.
procedure GAUSSIAN RANDOMIZATION($\mathbf{w}$)
  for $l = 1$ to L
    Generate $\boldsymbol{\zeta}_l \sim \mathcal{CN}(\mathbf{0}, \mathbf{W}^*)$;
    Construct a feasible solution $\mathbf{w}_l = \text{sgn}(\boldsymbol{\zeta}_l)/\sqrt{N_E}$;
  end for
  Determine $l^* = \max_{l=1,\ldots,L} \min_{1 \leq k \leq K} SIR_k(\mathbf{w}_l)$, where SIR_k is given by (54);
  $\mathbf{w}^* = \mathbf{w}_{l^*}$.

$$g_k(\mathbf{W}) = \sqrt{\sum_{l \neq k}^{K} \sum_{s,s'=1}^{N_{BS}} vec(\mathbf{W}^T)^T ({\mathbf{R}^E_{l,s's}}^T \otimes \mathbf{R}^E_{k,ss'}) vec(\mathbf{W})} \tag{64}$$

$$= || \left(\sum_{l \neq k}^{K} \sum_{s,s'=1}^{N_{BS}} ({\mathbf{R}^E_{l,s's}}^T \otimes \mathbf{R}^E_{k,ss'}) \right)^{\frac{1}{2}} vec(\mathbf{W}) ||_2. \tag{65}$$

It can be seen from (63) that $f_k(\mathbf{W})$ is a linear function of $\mathbf{W}$. Also $g_k(\mathbf{W})$ is a convex function, expressed as an L2 norm in (65). *Problem (P5)* therefore considers a set of ratios $\{\frac{f_k(\mathbf{W})}{g_k(\mathbf{W})}\}_{k=1}^K$, where each ratio has an affine numerator $f_k(\mathbf{W})$, convex denominator $g_k(\mathbf{W})$ and convex constraints and can therefore be solved using the generalized Dinkelbach's algorithm presented in Algorithm 6 of [37]. The Dinkelbach's procedure to solve *Problem (P5)* is formulated in **Algorithm 1**. Once the optimal $\mathbf{W}^*$ is obtained, the corresponding weight vector $\mathbf{w}$ that solves the *Problem (P3)* needs to be extracted. Generally the resulting matrix $\mathbf{W}^*$, although globally optimal for *Problem (P5)* has a rank greater than one and therefore yields a quasi-optimal solution for *Problem (P3)*. It is important to post-process the relaxed solution $\mathbf{W}^*$ to extract a close to

optimal $\mathbf{w}^*$. Besides the eigenvector approximation method, where $\mathbf{w}^*$ is approximated as the principal eigenvector of $\mathbf{W}^*$, randomization is another way to extract an approximate solution from the SDR solution $\mathbf{W}^*$. The idea is to generate a random vector $\boldsymbol{\zeta} \in \mathbb{C}^{N_E \times 1} \sim \mathcal{CN}(\mathbf{0}, \mathbf{W}^*)$ and use it to construct an approximate solution to *Problem (P3)*. The procedure and theoretical accuracy results have been discussed in [35], [39]. The specific design of the randomization procedure is problem-dependent and has been summarized at the end of **Algorithm 1**.

The proposed algorithm exploits the generalized Dinkelbach's algorithm to solve a sequence of convex problems with a linear convergence rate and obtain a SDR solution $\mathbf{W}^*$, from which a quasi-optimal weight vector $\mathbf{w}^*$ is obtained using the Gaussian randomization technique. Later, numerical results will confirm the excellent performance gains that can be obtained through this single optimal downtilt beamforming technique in the large (N_{BS}, N_E) regime. The proposed algorithm does not require the acquisition of high dimension CSI, since the weight vector is adapted using the quasi-static channel covariance matrices of the users.

V. User Group Specific Elevation Beamforming

In the last section, we discussed the single downtilt elevation beamforming scenario, where all the users are served by vertical beams transmitted using the same optimal downtilt antenna port weight vector, which maximizes the minimum SIR of the multi-user MISO system. However, the additional control over the elevation dimension in FD-MIMO systems enables a variety of strategies such as sector-specific and user-specific elevation beamforming [12].

In this section, we consider the user-group specific elevation beamforming scenario, where the user population is partitioned into groups based on their channel covariance matrices and each group is served by a set of antenna ports fed with the weight vector optimized for that particular user group. Different user groups are therefore served by different elevation domain beams. In order to effectively exploit this approach, the system must partition the user population into groups according to the following two qualitative principles from [40]; 1) users in the same group have channel covariance eigenspaces that approximately span a given common subspace, which characterizes the group; 2) the subspaces of groups served in the same time-frequency slot are approximately mutually orthogonal. There are several algorithms that achieve this grouping like the K-means clustering and fixed quantization algorithms. This section focuses on the latter.

In the fixed quantization grouping scheme, we consider G user groups, where the group subspaces denoted by $\mathbf{V}_g \in \mathbb{C}^{M \times r_g}; g = 1, \ldots G$, $M = N_{BS} \times N_E$, are fixed and known apriori

Algorithm 2 User Group Specific Elevation Beamforming

procedure USER GROUPING($\mathcal{S}_g$)
  for $g = 1$ to G
  Initialize the user group set $\mathcal{S}_g = \emptyset$;
  Choose $\theta_{0,g}$ and elevation spread $\triangle$ such that the intervals $[\theta_{0,g} - \triangle, \theta_{0,g} + \triangle]$ are disjoint;
  Compute $\mathbf{R}_g^E(\theta_{0,g}, \triangle)$ using (32) for the chosen $\theta_{0,g}$ and $\triangle$;
  Obtain the group subspace $\mathbf{V}_g = \mathbf{U}_g$, where $\mathbf{U}_g$ is the $M \times r_g$ tall matrix of eigenvectors corresponding to r_g dominant eigenvalues of $\mathbf{R}_g^E$, with r_g chosen such that $\sum_{g=1}^{G} r_g = M$;
  end for
  for $k = 1$ to K
  Compute $\mathbf{R}_k^E$ using (32) for the propagation scenario under study;
  Obtain the eigenspace $\mathbf{U}_k^{M \times r_k}$, corresponding to the r_k dominant eigenvalues of $\mathbf{R}_k^E$;
  Compute $d_C(\mathbf{U}_k, \mathbf{V}_g) = ||\mathbf{U}_k \mathbf{U}_k^H - \mathbf{V}_g \mathbf{V}_g^H||_F^2$;
  Find $g = \min_{1 \le g' \le G} d_c(\mathbf{U}_k, \mathbf{V}_{g'})$;
  Add user k to group g, i.e. $\mathcal{S}_g := \mathcal{S}_g \cup \{k\}$;
  end for
procedure WEIGHT VECTOR OPTIMIZATION($\mathbf{w}_g$)
  Divide N_{BS} antenna ports into G equal groups, with $N_{BS,g}$ ports serving each user group.
  for $g = 1$ to G
  Use **Algorithm 1** to obtain the quasi-optimal weight vector $\mathbf{w}_g^*$ for the antenna ports in group g serving the $\mathcal{S}_g$-user MISO system.
  end for

based on the geometric arrangement of the users in the cell. The performance of fixed quantization method depends critically on how these subspaces are chosen. The method employed here relies on the fact that in the large (N_{BS}, N_E) regime, the channel eigenspaces are approximately mutual orthogonal if the angular supports for the user groups are disjoint. Therefore, we choose G mean elevation AoDs, $\theta_{0,g}$, and a fixed value for the group elevation angular spread $\triangle$, such that the resulting intervals $[\theta_{0,g} - \triangle, \theta_{0,g} + \triangle]$ are disjoint. The $M \times M$ channel correlation matrices $\mathbf{R}_g^E$, $g = 1, \ldots G$, for these G sets of mean elevation AoDs and angular spread are formed using (32) and the corresponding eigenspaces $\mathbf{V}_g$, $g = 1, \ldots G$, are computed. The K users are then

assigned to these G groups, based on the chordal distance between the user channel correlation eigenspaces and the group subspaces. The number of users in each group is denoted by K_g. This form of grouping is implemented using the slowly-varying channel correlation matrices of the users, requiring only the knowledge of the mean AoDs/AoAs and the angular spreads.

At the transmitter side, the antenna ports are partitioned into G groups, where the number of antenna ports in each group is $N_{BS,g} = N_{BS}/G$, where G is chosen as a factor of N_{BS}. The first $N_{BS,g}$ adjacent ports in Fig. 2 serve the first user group and so on. The optimal weight vector for the g^{th} antenna port group, $\mathbf{w}_g^*$, is obtained using **Algorithm 1**, utilizing the channel correlation matrices of the users in the g^{th} group. Therefore G different elevation beams are designed. The user group specific elevation beamforming technique is summarized in **Algorithm 2** and will be shown to yield excellent performance gains in the next section in the large (N_{BS}, N_E) regime.

VI. Results and Discussions

The performance gains realizable through careful design of the downtilt weight vectors is now studied using simulations. The 3D-urban macro cell environment from [6] is adopted with parameters set as $\theta_{3dB}, \phi_{3dB} = 65^o$, $\sigma_t = 15^o$, $\kappa_t = 10$, $\mu = 0$ and $G_{E,max} = 8$dBi.

The single-user MISO case is studied first, where **Theorem 2** is used to optimize the weight vectors $\mathbf{w}_s$, $s = 1, \ldots, N_{BS}$, for the antenna ports. The BS equipped with a $10 \times N_{BS}$ AAS serves an outdoor user located at the edge of a cell of radius $250m$, with θ_0 for this user computed to be 95.37^o. The user throughput for the optimal downtilt weight vectors is plotted in red in Fig. 7 along with the cases where the electrical downtilt angles are set to specific pre-defined values with weights computed using (9) for $\phi_{scan} = 0^o$. It is evident that choosing the weight vectors according to **Theorem 2** yields higher user throughput. Since $\theta_0 = 95.37^o$, the cases where θ_{tilt} is set to 90^o and 100^o achieve approximately the same performance, whereas the performance for other downtilt angles deteriorates severely. Also, the theoretical throughput obtained using (69) approximates the Monte-Carlo simulated throughput obtained using (39) quite well.

The multi-user MISO system is studied next where K users are placed randomly in a cell of radius $250m$, at a minimum distance of $50m$ from the BS. A 10×40 AAS is employed. The optimal weight vector for the antenna ports maximizing the minimum SIR_k, $k = 1, \ldots K$ is obtained through **Algorithm 1**, utilizing the user channel covariance matrices computed using (30). The Monte-Carlo simulated minimum SIR_k in (49) is plotted in Fig. 8 along with the deterministic equivalent in (51) for the quasi-optimal weight vector $\mathbf{w}^*$, under the assumption

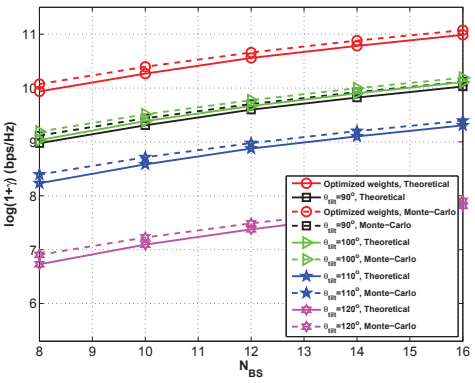

Fig. 7. Performance of a single user MISO system.

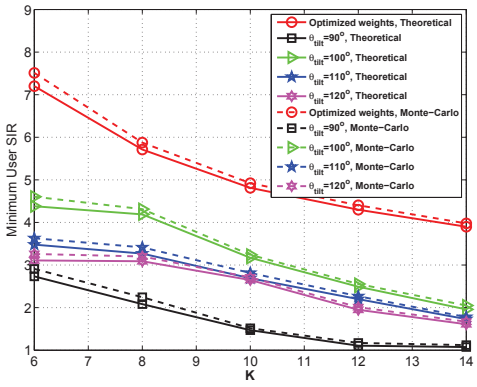

Fig. 8. Performance of a multi-user MISO system.

that all ports transmit using the same downtilt weight vector. The results for the weight vector computed using (9) for pre-defined downtilt values are also plotted. The deterministic equivalent in **Proposition 1** matches the Monte-Carlo result quite well for moderate number of antennas. More importantly, the potential of elevation beamforming in enhancing the system performance is confirmed through this result. Even the single optimal downtilt beamforming scenario achieves significant performance gains as compared to the cases where the downtilt angle is pre-defined.

Next, we study the performance of user group-specific elevation beamforming, where K users are divided into G groups based on their channel correlation matrices and group subspaces. The antenna ports are divided into G groups too, where the ports in each group are applied with the same downtilt weight vector optimized using the statistics of the users being served in that group. The simulation is done for $N_{BS} = 36$, $N_E = 5$ and $G = 3$. The values for $\theta_{0,g}$, $g = 1, \ldots, G$ and $\triangle$ are set as $[93^o, 101^o, 119^o]$ and 7.8^o respectively such that the resulting intervals $[\theta_{0,g} - \triangle, \theta_{0,g} + \triangle]$ are disjoint. The user grouping is done as explained in **Algorithm 2**, where $r_g^* = 60$ and the optimal weight vector for each $N_{BS,g} = 12$ antenna ports group, $\mathbf{w}_g^*$, $g = 1, \ldots, G$, is computed using **Algorithm 1**. The result for the minimum user SIR is plotted in Fig. 9, which clearly highlights the superior performance of the user-grouping algorithm. The gap between the curves with and without grouping starts to decrease as K increases, because for higher K, a larger number of users K_g are served in each group by the same $N_{BS,g}$ antenna ports per group. In fact, when the values N_{BS} and K are comparable, the arrangement of the users could be such that the number of users in one of the g groups, $K_g > N_{BS,g}$, while the overall number of users $K < N_{BS}$, resulting in a degradation of the minimum SIR under grouping.

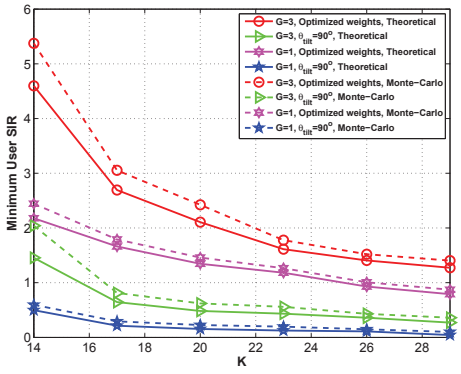

Fig. 9. Performance of user-group specific elevation beamforming in a multi-user MISO system.

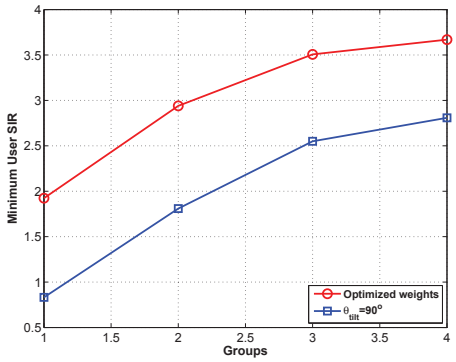

Fig. 10. Effect of the number of user groups on the performance of a multi-user MISO system.

In the next figure, we study the effect of increasing the number of user groups. The results are plotted for $G = 2, 3$ and 4 in Fig. 10, where $\theta_{0,g}$, $g = 1, \ldots, G$ and $\triangle$ are selected, ensuring that the resulting angular supports are disjoint. A 3×48 AAS is utilized for $K = 22$ users. Following the steps in **Algorithm 2**, the quasi-optimal weight vector $\mathbf{w}_g^*$, for each antenna ports group g serving the g^{th} user group, $g = 1, \ldots, G$, is computed. The result shows that the higher is the number of groups, the larger is the performance gain, since every user group is now served with an optimal downtilt weight vector determined using the spatial statistics of only the users in that group. A higher number of groups realizes a higher degree of vertical separation of the users through the design of a higher number of elevation domain beams, where each beam serves a small number of co-located users. Note that the value of N_{BS} needs to be high enough, such that $N_{BS,g} >> K_g$, even after dividing the ports and the users into G groups.

These founding results provide a flavor of the performance gains realizable through the deployment of an AAS with a 2D planar array structure at the BS, where every antenna port is fed with a corresponding downtilt weight vector to realize spatially separated transmissions to a large number of users. More sophisticated 3D beamforming techniques can be devised in the future that allow every port to transmit at a different optimal downtilt angle. In fact, for $N_{BS} >> K$, spatially separated beams to almost all the users can be realized, which is why FD beamforming can be highly advantageous when amalgamated with massive MIMO techniques.

VII. Conclusion

This paper reviewed the recent development of FD-MIMO technology for evolution towards 5G cellular systems and studied the architecture of the 2D active antenna arrays utilized by these

systems. The 2D AAS not only serves as a practical implementation of massive MIMO systems, but also offers the potential to boost spectral efficiency by providing the ability of adaptive electronic beam control in both the elevation and azimuth dimensions. To facilitate the evaluation of these systems, the recently proposed 3D channel model in the 3GPP TR36.873 was outlined. The SCF for the channels constituted by individual antenna elements in the AAS was derived and used to compute the correlation between overall antenna ports for any arbitrary 3D propagation environment. The performance benefits of FD-MIMO techniques were then studied by devising elevation beamforming algorithms, that optimize the downtilt antenna port weight vectors in the single user and multi-user MISO settings, utilizing the quasi-static channel correlation matrices of the users obtained from the derived SCF. The problem of determining the downtilt weight vector that maximizes the minimum SIR of the multi-user system was formulated under the assumption that all ports serve using the same optimal downtilt weight vector, and solved using SDR and Dinkelbach's method. Finally, the user-group specific elevation beamforming scenario was devised. Simulation results confirmed the potential of FD-MIMO techniques to improve the system performance. In this paper, we focused on the single-cell scenario for the sake of clarity and space limitation. As a future work, it is of interest to develop 3D beamforming algorithms for the multi-cell case. The objective function will now take into consideration the out-of-cell interference making the joint max-min problem harder. However, the quasi-optimal weight vectors can be designed by implementing Algorithm 1 in a distributed iterative manner.

APPENDIX A
PROOF OF THEOREM 2

This theorem follows from expressing $tr(\mathbf{h}\mathbf{h}^H)$ as a quadratic term in $\mathbf{z}$ using (34) to re-write the SNR in (39) as follows,

$$\gamma = \frac{\varrho}{\sigma_n^2}\mathbf{h}^H\mathbf{h} = \frac{\varrho}{\sigma_n^2}\mathbf{z}^H{\mathbf{R}_{BS}^{\frac{1}{2}}}^H\mathbf{R}_{BS}^{\frac{1}{2}}\mathbf{z}. \tag{66}$$

Next exploiting **Lemma 2** and the fact that the covariance matrix $\mathbf{R}_{BS}$ defined in (30) is Hermitian, positive semi-definite and satisfies the condition in Assumption A-1 we have,

$$\frac{1}{N_{BS}}\mathbf{z}^H\mathbf{R}_{BS}\mathbf{z} - \frac{1}{N_{BS}}tr(\mathbf{R}_{BS}) \xrightarrow{a.s.} 0. \tag{67}$$

$$\text{where,} \quad tr(\mathbf{R}_{BS}) = \sum_{s=1}^{N_{BS}} {\mathbf{w}_s}^H\mathbf{R}_{ss}^E\mathbf{w}_s, \tag{68}$$

and $\mathbf{R}_{ss}^E$ is a $N_E \times N_E$ matrix given by $\mathbf{R}^E([(s-1)N_E+1 : sN_E], [(s-1)N_E+1 : sN_E])$,

where $\mathbf{R}^E$ is defined in (32). Therefore in the large (N_{BS}, N_E) regime,

$$\frac{1}{N_{BS}}\gamma - \frac{\varrho}{N_{BS}\sigma_n^2}\sum_{s=1}^{N_{BS}} \mathbf{w}_s{}^H \mathbf{R}_{ss}^E \mathbf{w}_s \xrightarrow{a.s.} 0. \tag{69}$$

Consequently, in the large (N_{BS}, N_E) regime, the optimization problem (*P1*) can be written as,

$$\underset{\mathbf{w}_1,\mathbf{w}_2,\ldots,\mathbf{w}_{N_{BS}}}{\text{maximize}} \sum_{s=1}^{N_{BS}} \mathbf{w}_s{}^H \mathbf{R}_{ss}^E \mathbf{w}_s \tag{70}$$

$$\text{subject to } ||\mathbf{w}_s||_2 = 1, \text{ for } s = 1, \ldots, N_{BS}. \tag{71}$$

Problem (*P1*) is equivalent to finding the optimal $\mathbf{w}_s^*$= $\arg\max_{\mathbf{w}\ ||\mathbf{w}||_2=1} ||\mathbf{R}_{ss}^{E\ \frac{1}{2}}\mathbf{w}||_2^2$, $s = 1, \ldots, N_{BS}$, which has the simple eigenvector solution stated in **Theorem 2**.

APPENDIX B
PROOF OF PROPOSITION 1

In order to prove **Proposition 1**, the following theorem will be required.

Theorem 3. Continuous Mapping Theorem [41]. Let $\{X_n\}$ be a sequence of N-dimensional random vectors. Let $g : \mathbb{R}^N \to \mathbb{R}^L$ be a continuous function. Then,

$$X_n \xrightarrow{a.s.} X \Longrightarrow g(X_n) \xrightarrow{a.s.} g(X), \tag{72}$$

where $\xrightarrow{a.s.}$ denotes almost sure convergence.

To prove **Proposition 1**, note that the channel vector for user k, $\mathbf{h}_k$ is given by $\mathbf{R}_{BS_k}^{\frac{1}{2}}\mathbf{z}_k$, where the condition described in **Assumption A-1** on the Hermitian, positive semi-definite channel covariance matrices $\mathbf{R}_{BSk}$ hold for all users, $k = 1, \ldots, K$. With this, (49) can be written as,

$$SIR_k = \frac{|\mathbf{z}_k^H \mathbf{R}_{BSk} \mathbf{z}_k|^2}{\sum_{l\neq k}^K \mathbf{z}_k^H \mathbf{R}_{BS_k}^{\frac{1}{2}\ H} \mathbf{h}_l \mathbf{h}_l^H \mathbf{R}_{BS_k}^{\frac{1}{2}} \mathbf{z}_k}. \tag{73}$$

Applying **Lemma 2** along with the continuous mapping theorem on the numerator and **Lemma 2** along with the fact that if $\mathbf{A} \in \mathbb{C}^{M\times N}$ and $\mathbf{B} \in \mathbb{C}^{N\times M}$, then $tr(\mathbf{AB}) = tr(\mathbf{BA})$ would yield the following convergence result for (73),

$$\frac{1}{N_{BS}} SIR_k - \frac{(\frac{1}{N_{BS}} tr(\mathbf{R}_{BSk}))^2}{\sum_{l\neq k}^K \frac{1}{N_{BS}} tr(\mathbf{R}_{BSk}\mathbf{h}_l\mathbf{h}_l^H)} \xrightarrow{a.s.} 0. \tag{74}$$

Substituting the expression for $\mathbf{h}_l$ as $\mathbf{R}_{BS_l}^{\frac{1}{2}}\mathbf{z}_l$ and applying the convergence theorem in **Lemma 2** a second time on the denominator would yield,

$$SIR_k - \frac{(\frac{1}{N_{BS}} tr(\mathbf{R}_{BSk}))^2}{\sum_{l\neq k}^K \frac{1}{N_{BS}^2} tr(\mathbf{R}_{BS_l}^{\frac{1}{2}\ H} \mathbf{R}_{BSk} \mathbf{R}_{BS_l}^{\frac{1}{2}})} \xrightarrow{a.s.} 0. \tag{75}$$

Again using $tr(\mathbf{AB}) = tr(\mathbf{BA})$, would complete the proof of **Proposition 1**.

REFERENCES

[1] E. Dahlman, S. Parkvall, J. Sköld, and P. Beming, *3G Evolution, Second Edition: HSPA and LTE for Mobile Broadband*, 2nd ed. Academic Press, 2008.

[2] F. Rusek, D. Persson *et al.*, "Scaling up MIMO: Opportunities and challenges with very large arrays," *IEEE Signal Processing Magazine*, vol. 30, no. 1, pp. 40–60, Jan. 2013.

[3] T. L. Marzetta, "Noncooperative cellular wireless with unlimited numbers of base station antennas," *IEEE Transactions on Wireless Communications*, vol. 9, no. 11, pp. 3590–3600, November 2010.

[4] L. Lu, G. Y. Li, A. L. Swindlehurst, A. Ashikhmin, and R. Zhang, "An overview of massive MIMO: Benefits and challenges," *IEEE Journal of Selected Topics in Signal Processing*, vol. 8, no. 5, pp. 742–758, Oct. 2014.

[5] Y. H. Nam, B. L. Ng, K. Sayana, Y. Li, J. Zhang, Y. Kim, and J. Lee, "Full-dimension MIMO (FD-MIMO) for next generation cellular technology," *IEEE Communications Magazine*, vol. 51, no. 6, pp. 172–179, June 2013.

[6] 3GPP TR 36.873 V12.0.0, "Study on 3D channel model for LTE," Sep. 2014.

[7] 3GPP TR 37.840 V12.00, "Study of radio frequency (RF) and electromagnetic compatibility (EMC) requirements for active antenna array system (AAS) base station," Mar. 2013.

[8] K. Linehan and R. Chandrasekaran, "Active antennas: The next step in radio and antenna evolution," [Online]. Available: https://www.yumpu.com/en/document/view/8991085/active-antennas-the-next-step-in-radio-and-antenna-evolution.

[9] Huawei, "Active antenna system: Utilizing the full potential of radio sources in the spatial domain," [Online]. Available: http://www1.huawei.com/en/static/AAS-129092-1-197969.pdf, Nov. 2012.

[10] R1-122034, "Study on 3D channel Model for elevation beamforming and FD-MIMO studies for LTE," 3GPP TSG RAN Plenary no. 58, Barcelona, Spain, Dec. 2012.

[11] 3GPP TR 36.897 V13.0.0 , "Study on elevation beamforming/Full-Dimension (FD) MIMO for LTE ," June 2015.

[12] Y. Song, X. Yun, S. Nagata, and L. Chen, "Investigation on elevation beamforming for future LTE-Advanced," in *2013 IEEE International Conference on Communications Workshops (ICC)*, June 2013, pp. 106–110.

[13] A. Kammoun, H. Khanfir, Z. Altman, M. Debbah, and M. Kamoun, "Preliminary results on 3D channel modeling: From theory to standardization," *IEEE Journal on Selected Areas in Communications*, vol. 32, no. 6, pp. 1219–1229, June. 2014.

[14] W. Lee, S. R. Lee, H.-B. Kong, and I. Lee, "3D beamforming designs for single user MISO systems," in *2013 IEEE Global Communications Conference (GLOBECOM)*, Dec 2013, pp. 3914–3919.

[15] Y. Kim, H. Ji, J. Lee, Y. H. Nam, B. L. Ng, I. Tzanidis, Y. Li, and J. Zhang, "Full dimension MIMO (FD-MIMO): the next evolution of MIMO in LTE systems," *IEEE Wireless Communications*, vol. 21, no. 2, pp. 26–33, April 2014.

[16] J. Koppenborg, H. Halbauer, S. Saur, and C. Hoek, "3D beamforming trials with an active antenna array," in *Proc. ITG Workshop on Smart Antennas*, 2012, pp. 110–114.

[17] S. Saur and H. Halbauer, "Exploring the vertical dimension of dynamic beam steering," in *2011 8th International Workshop on Multi-Carrier Systems & Solutions (MC-SS)*, May 2011, pp. 1–5.

[18] RP-141831, "Revised SID: Study on elevation beamforming/full-Dimension (FD) MIMO for LTE," Samsung, Nokia Networks, 2014.

[19] Radiocommunication Sector of International Telecommunication Union, "Report ITU-R M.2135-1: Guidelines for evaluation of radio interface technologies for IMT-advanced," 2009.

[20] 3GPP TR 36.814 V9.0.0 , "Further advancements for E-UTRA physical layer aspects (Release 9)," March 2010.

[21] B. Partov, D. J. Leith, and R. Razavi, "Utility fair optimization of antenna tilt angles in LTE networks," *IEEE/ACM Transactions on Networking*, vol. 23, no. 1, pp. 175–185, Feb. 2015.

[22] N. Seifi, J. Zhang, R. W. Heath, T. Svensson, and M. Coldrey, "Coordinated 3D beamforming for interference management in cellular networks," *IEEE Transactions on Wireless Communications*, vol. 13, no. 10, pp. 5396–5410, Oct. 2014.

[23] S. K. Yong and J. Thompson, "Three-dimensional spatial fading correlation models for compact MIMO receivers," *IEEE Transactions on Wireless Communications*, vol. 4, no. 6, pp. 2856–2869, Nov. 2005.

[24] M. Shafi, M. Zhang, A. L. Moustakas, P. J. Smith, A. F. Molisch, F. Tufvesson, and S. H. Simon, "Polarized MIMO channels in 3D: Models, measurements and mutual information," *IEEE Journal on Selected Areas in Communications*, vol. 24, no. 3, pp. 514–527, 2006.

[25] K. Mammasis, R. Stewart, and J. Thompson, "Spatial fading correlation model using mixtures of von mises fisher distributions," *IEEE Transactions on Wireless Communications*, vol. 8, no. 4, pp. 2046–2055, April. 2009.

[26] P. D. Teal, T. D. Abhayapala, and R. A. Kennedy, "Spatial correlation for general distributions of scatterers," *IEEE Signal Processing Letters*, vol. 9, no. 10, pp. 305–308, Oct. 2002.

[27] W. Zhang, J. Xiang *et al.*, "Field trial and future enhancements for TDD massive MIMO networks," in *IEEE 26th International Symposium on Personal, Indoor, and Mobile Radio Communications (PIMRC)*, Aug. 2015, pp. 2339–2343.

[28] D. Colton and R. Kress, *Inverse Acoustic and Electromagnetic Scattering Theory*, 3rd ed. New York, NY: Springer, 2013.

[29] D. J. Hofsommer and M. L. Potters, "Table of fourier coefficients of assosciated legendre functions," R 478 Computation Department of the Mathematical Center, Amsterdam, June 1960.

[30] Q.-U.-A. Nadeem, A. Kammoun, M. Debbah, and M.-S. Alouini, "A generalized spatial correlation model for 3D MIMO channels based on the fourier coefficients of power spectrums," *IEEE Transactions on Signal Processing*, vol. 63, no. 14, pp. 3671–3686, July 2015.

[31] ——, "Spatial correlation characterization of a full dimension massive MIMO system," in *2016 IEEE Global Communications Conference: Wireless Communications (Globecom2016 WC)*, Dec. 2016.

[32] E. Björnson, J. Hoydis, M. Kountouris, and M. Debbah, "Massive MIMO systems with non-ideal hardware: Energy efficiency, estimation, and capacity limits," *IEEE Transactions on Information Theory*, vol. 60, no. 11, pp. 7112–7139, Nov. 2014.

[33] R. Couillet and M. Debbah, *Random matrix methods for wireless communications*, 1st ed. New York, NY, USA: Cambridge University Press, 2011.

[34] T. K. Y. Lo, "Maximum ratio transmission," *IEEE Transactions on Communications*, vol. 47, no. 10, pp. 1458–1461, Oct. 1999.

[35] E. Karipidis, N. D. Sidiropoulos, and Z. Q. Luo, "Quality of service and max-min fair transmit beamforming to multiple cochannel multicast groups," *IEEE Transactions on Signal Processing*, vol. 56, no. 3, pp. 1268–1279, March 2008.

[36] A. Zappone and E. Jorswieck, "Energy efficiency in wireless networks via fractional programming theory," *Foundations and Trends in Communications and Information Theory*, vol. 11, no. 3-4, pp. 185–396, 2015.

[37] A. Zappone, L. Sanguinetti, G. Bacci, E. Jorswieck, and M. Debbah, "Energy-efficient power control: A look at 5G wireless technologies," *IEEE Transactions on Signal Processing*, vol. 64, no. 7, pp. 1668–1683, April 2016.

[38] K. Schäcke, "On the kronecker product," Masters Thesis, University of Waterloo, 2013.

[39] Z. Q. Luo, W. K. Ma, A. M. C. So, Y. Ye, and S. Zhang, "Semidefinite relaxation of quadratic optimization problems," *IEEE Signal Processing Magazine*, vol. 27, no. 3, pp. 20–34, May 2010.

[40] J. Nam, A. Adhikary, J. Y. Ahn, and G. Caire, "Joint spatial division and multiplexing: Opportunistic beamforming, user grouping and simplified downlink scheduling," *IEEE Journal of Selected Topics in Signal Processing*, vol. 8, no. 5, pp. 876–890, Oct. 2014.

[41] J. Shao, *Mathematical statistics*. New York, NY, USA: Springer, 2007.